Food Hydrocolloids 89 (2019) 67–79

Contents lists available at ScienceDirect

Food Hydrocolloids

journal homepage: www.elsevier.com/locate/foodhyd

Characterization of biodegradable/non-compostable films made from cellulose acetate/corn starch blends processed under reactive extrusion conditions

Clémence Herniou–Julien[a], Julieta R. Mendieta[b], Tomy J. Gutiérrez[c,*]

[a] Faculté Sciences & Sciences de l'ingénieur, Université de Bretagne-Sud (UBS), 2 rue Coat Saint-Haouen, 56100 Lorient, France
[b] Grupo de Fisiología del Estrés en Plantas, Instituto de Investigaciones Biológicas (IIB), Facultad de Ciencias Exactas y Naturales, Universidad Nacional de Mar del Plata (UNMdP), Consejo Nacional de Investigaciones Científicas y Técnicas (CONICET) y Comisión de Investigaciones Científicas (CIC), Deán Funes 3250, B7602AYJ, Mar del Plata, Argentina
[c] Grupo de Materiales Compuestos Termoplásticos (CoMP), Instituto de Investigaciones en Ciencia y Tecnología de Materiales (INTEMA), Facultad de Ingeniería, Universidad Nacional de Mar del Plata (UNMdP) y Consejo Nacional de Investigaciones Científicas y Técnicas (CONICET), Colón 10850, B7608FLC, Mar del Plata, Argentina

ARTICLE INFO

Keywords:
Active films
Biodegradability
Compostability
Cross-linking
Shape memory films
Thermoplastic starch

ABSTRACT

The manufacture of food packaging materials from food hydrocolloids has been widely studied during the last decades and multiple alternatives have been investigated, with research mainly focusing on improving the physicochemical and mechanical properties of the different materials. Processing food hydrocolloids by reactive extrusion (REx) for the development of food packaging has, however, been poorly studied. Four film systems were prepared from corn (*Zea mays*) thermoplastic starch (TPS) containing either cellulose acetate (C) or chromium octanoate (Cat - a potential food grade catalyst), or a blend of both (C + Cat). Processing was done under REx conditions using a twin-screw extruder. An exhaustive study of the resulting materials was carried out in terms of the structural, physicochemical, thermal, surface, mechanical and compostable properties related to their potential use in food packaging applications. The most hydrophobic material was the C-containing film. However, this physicochemical behavior was different on the film surface, thus suggesting molecular rearrangements within the material. The Cat-containing films were darker than the other materials. The mechanical behavior observed in the Cat-containing films was particularly interesting as it suggests that these film systems could be used as shape memory materials for food packaging applications, as long as the following mechanical conditions are not exceeded: 5.02% strain and 0.43 MPa stress. All the films tested were biodegradable. We confirmed that Cat-containing film systems produced non-compostable materials at high concentrations (1 mg/mL), as measured by its effect on lettuce seedlings. This confirms that biodegradable materials are not necessarily compostable.

1. Introduction

The development of edible films derived from different food hydrocolloids (starch, cellulose, proteins, and gums) for their use as food packaging materials has been extensively studied over the last two decades with the aim to replace synthetic polymers obtained from the petrochemical industry (Gutiérrez & Alvarez, 2018). The mechanical, thermal and physicochemical characteristics of different food hydrocolloid matrices with several types of nano-fillers intentionally added has also been widely investigated in order to improve their mechanical properties, reduce water susceptibility, and develop active and "intelligent" (A&I) edible polymers for food packaging systems (Gutiérrez, 2018a; Gutiérrez, González Seligra, Medina Jaramillo, Famá, & Goyanes, 2017). These studies have, however, often been conducted using the casting methodology, which has proved to be most efficient for the preliminary study of novel matrices or to undertake specific studies that are well suited to a laboratory scale (Chevalier, Assezat, Prochazka, & Oulahal, 2018). It has become more and more necessary, however, to undertake scientific studies that really satisfy the needs of society and industry, in other words studies that, provide results that are applicable after technological scaling. For this reason, scientific studies of food hydrocolloids processed by industrial scale

* Corresponding author. Institute of Research in Materials Science and Technology, Faculty of Engineering, National University of Mar del Plata and National Scientific and Technical Research Council (CONICET), PO Box B7608FLC, Colón 10850, Mar del Plata, Argentina.
E-mail addresses: tomy.gutierrez@fi.mdp.edu.ar, tomy_gutierrez@yahoo.es (T.J. Gutiérrez).

https://doi.org/10.1016/j.foodhyd.2018.10.024
Received 8 September 2018; Received in revised form 14 October 2018; Accepted 15 October 2018
Available online 20 October 2018
0268-005X/ © 2018 Elsevier Ltd. All rights reserved.

methodologies such as blown extrusion, compression or injection molding are well received. Taking all this into account, this study has been designed using extrusion, a processing methodology frequently found in the polymer and food industry (Gutiérrez & Alvarez, 2018). Extrusion processing not only has the advantage of being a continuous system, but also, due to the high pressures and temperatures that can be reached, enables the equipment to behave like a reactor. Hence, under the processing conditions used and depending on the characteristics of the polymer blends, reactive extrusion (REx) can be achieved (Gutiérrez, Guarás, & Alvarez, 2017b).

In principle, REx aims to achieve cross-linking reactions between polymers or polymers/nano-fillers. Cross-linking minimizes phase separation between polymers and/or improves adhesion between the polymer matrix and the nano-fillers, resulting in food packaging materials with improved properties. Recent studies carried out by our research group have focused on the investigation of octanoates as catalysts that promote cross-linking reactions between polymers processed by extrusion (Gutierrez & Alvarez, 2017a; 2017b, 2017c). For example, we have demonstrated that the zinc and zirconium octanoates are not only effective as catalysts, but also remain within the polymer matrix after the cross-linking reactions have occurred and impart it with antimicrobial properties against both Gram positive and Gram negative bacteria. Thus, these octanoates fulfill a dual function of catalyst plus broad spectrum antimicrobial agent resulting in active films (Gutiérrez & Alvarez, 2017b, 2017c). The main reason for using octanoates as catalysts is that some, e.g. tin octanoate ($Sn(Oct)_2$), are already widely used (Kowalski, Duda, & Penczek, 1998) and have been approved as food additives by the U.S. Food and Drug Administration (FDA, 2016).

REx of synthetic polymer/starch blends (Gutiérrez & Alvarez, 2017c; Liu, Xie, Yu, Chen, & Li, 2009; Yu, Dean, & Li, 2006), as well as synthetic polymer/cellulose blends has already been well studied (Dai et al., 2015; Dai, Xiong, Na, & Zhu, 2014; Dhar, Tarafder, Kumar, & Katiyar, 2016; Dogu & Kaynak, 2016; Khoo & Chow, 2017; Morelli, Belgacem, Bretas, & Bras, 2016; Zhang & Zhang, 2016). Nonetheless, REx of food hydrocolloids such as starch and cellulose derivatives has not been yet evaluated. Furthermore, it is not clear from the literature if the octanoate catalysts also promote cross-linking reactions in thermoplastic starch (TPS) chains, since until now they have only been used to catalyze cross-linking reactions between synthetic polymers and starch.

On another note, we also wanted to investigate the compostability of these types of materials since, a biodegradable material is not necessarily compostable (Gutiérrez, 2018b, 2018c). In addition, the compostability of starch-based food packaging materials has been little studied in the published literature.

With this in mind, films made from blending two food hydrocolloids derived from abundant and ubiquitous natural polymers, corn starch and cellulose acetate, were processed under REx conditions followed by thermo-molding. The films were characterized and analyzed exhaustively in order to determine cross-linking reactions between 1) the starch chains themselves, 2) the starch-cellulose acetate blend. Finally, the biodegradability and compostability of the materials were also investigated.

2. Experimental

2.1. Materials

Corn starch (*Zea mays*), glycerol, and cellulose acetate (C) were used as the polymer matrix, plasticizer and filler, respectively, in the preparation of the films. Corn starch was purchased from the Distribuidora Dos Hermanos, Mark Ying Yang (Mar del Plata, Argentina). Glycerol (density = 1.26 g/mL; boiling point = 290 °C) was obtained from Aurum (Mar del Plata, Argentina). C powder with a typical molar weight (M_w) of 30,000 g/mol (determined by gel permeation chromatography, GPC), 39.8 wt% acetyl content and maximum thermal degradation temperature 367 °C (Appendix A) was purchased from Aldrich (product code: 180955-500G). The catalyst (chromium(III) 2-ethylhexanoate [IUPAC name] - chromium octanoate [trade name] - Cr $(C_8H_{15}O_2)_3$ [molecular formula] - $Cr(Oct)_3$ [condensed molecular formula]; density = 1.01 g/mL at 25 °C, and boiling point = 142 °C at 760 mmHg) (Appendix A) was kindly provided by Ghion, Laboratorios Químicos, S.R.L. (Mar del Plata, Argentina). The FTIR spectra and TGA curves for C and the catalyst (Cat) are also provided in Appendix A.

2.2. Film formation & extrusion conditions

All the film systems were developed using a 56:190 (g/g) ratio (glycerol:starch). A similar glycerol:starch ratio was used by Toro-Márquez, Merino, and Gutiérrez (2018). To evaluate the effects of adding C and Cat to the starch matrix they were added separately to give two film systems: 19 g (10% w/w with respect to starch content) of C or 7 mL (3.68% v/w with respect to starch matrix) of Cat. A blend containing C and Cat was also prepared, maintaining the same amounts as before. The percent C employed was based on studies carried out by other authors who evaluated the effects of 0–20% nanocellulose content in potato starch-based films (Morán, Vázquez, & Cyras, 2013): no statistically significant differences were observed for percentages greater than 10% w/w. In this study, the catalyst concentration was slightly higher than that used by our research group to crosslink corn starch/polystyrene (1.9% zinc octanoate) and plantain flour/poly(ε-caprolactone) (PCL) (3.3% zirconium octanoate) (Gutierrez & Alvarez, 2017a; 2017b, 2017c). This was done with the purpose of trying to guarantee the potential cross-linking effect on the food hydrocolloid matrices used in this study. Each film system was pre-blended manually until homogeneous mixtures were obtained. The mixtures were then processed by extrusion in a twin-screw extruder with six heating zones. The temperature profile used was 90/100/105/110/120/120 °C with a screw rotation speed of 30 Hz and feed rate 15 g/min. These extrusion conditions were based on a previous study carried out by our research group (Gutiérrez & Alvarez, 2018). After processing, the materials obtained from the extruder were allowed to cool to room temperature (25 °C) before being pelletized using an automatic pelletizer (Weinuo Technology Co., Ltd., Jiangsu, China). The pellets (90 g per film system) were then hot-pressed using a hydraulic press (Proflow, Mar del Plata, Argentina) at 130 °C and 5×10^6 Pa (50 bar) for 10 min, after which a cooling cycle was applied until they reached a temperature of 30 °C. The four resulting materials were labeled as follows: thermoplastic starch (TPS), TPS + C, TPS + Cat and TPS + C + Cat. Finally, the prepared films were conditioned under controlled relative humidity (RH, ~57%) for a week at 25 °C before characterization.

2.3. Film characterization

2.3.1. Attenuated total reflectance Fourier transform infrared (ATR/FTIR) spectroscopy

Infrared spectra of the film samples were obtained from a Nicolet 6700 FTIR spectrometer (Thermo Scientific Instrument Co., Madison, Wisconsin, USA) using the single reflection horizontal ATR accessory Smart Orbit, and a diamond crystal at an incident angle of 45°. The FTIR spectra were acquired in the range of 400–4000 cm^{-1} from 32 co-added scans at 4 cm^{-1} resolution and were used to identify potential chemical interactions or the formation of new bonds. The ratio between the absorbance at 3300 cm^{-1} (A_{3300}) and 1150 cm^{-1} (A_{1150}), (A_{3300}/A_{1150} ratio) was also used to compare the number of available OH group in these types of film system following Shi et al. (2007). Each sample was scanned twice, observing good reproducibility.

2.3.2. Moisture content (MC), water solubility (WS), water absorption (WA), swelling (SW) & surface moisture (SM)

The MC of the different film systems was calculated using the methodology described by AOAC (1990) and the following equation:

$$MC\ (\%) = \frac{W_w - W_d}{W_w}\ x\ 100 \quad (1)$$

where W_w is the wet weight and W_d the dry weight of each film system. The dry weight of the films was determined by cutting samples of each system into 2 cm × 2 cm pieces, heating them in an oven at 105 °C for 24 h, and then weighing each one with an analytical balance (Denver Instrument APX-200). Analyses were performed in triplicate and the MC (%) ± standard deviation (SD) was reported.

To determine the WS percentages three replicates of each film system were cut into 2 cm × 2 cm pieces. The initial dry weight (W_i) of each film type was then determined by drying the pieces to a constant weight in an oven (Memmert, Germany) at 105 °C for 24 h. Each sample was then immersed in 50 mL of distilled water and kept at 25 °C for 24 h. The insoluble portions of the film samples were separated from the soluble matter in the water and dried in an oven at 105 °C for 24 h. The oven dried samples were then reweighed to measure the weight of the unsolubilized dry matter (W_f). The data obtained was used to calculate the WS for each film system using Eq. (2):

$$WS\ (\%) = \frac{(W_i - W_f)}{W_i}\ x\ 100 \quad (2)$$

The WA of the developed films was measured following the methodology proposed by Ludueña, Vázquez, and Alvarez (2012), with some modifications. Samples of each film system were cut into 2 cm × 2 cm pieces and dried in an oven at 105 °C for 24 h. The dry film pieces were then placed in containers with controlled RH (~57%). The tests were carried out under controlled temperature (25 °C) and pressure (1 atm). The WA was then calculated using Eq. (3):

$$WA\ (\%) = \frac{(W_{t=24h} - W_{t=0})}{W_{t=0}}\ x\ 100 \quad (3)$$

where $W_{t=0}$ is the initial dry weight, and $W_{t=24h}$ the final weight after 24 h (stationary state) of the films.

The SW percentage of films was determined according to the method described by Liu et al. (2017). Samples of each film type were initially cut into 11 mm diameter ($ø_i$) discs. Film discs were dried before immersion in containers with 20 mL distilled water. The containers were then sealed and maintained at 25 °C for 24 h. Changes in the disc diameters ($ø_f$) of the samples were recorded with the aid of an 8.1 mega-pixel Cyber-shot Sony camera, model DSC-H3 (Japan). At least three samples of each film system were tested to ensure good reproducibility and the SW (%) ± SD was reported. SW was calculated using Eq. (4):

$$SW\ (\%) = (ø_f - ø_i) * ø_i^{-1} * 100 \quad (4)$$

To estimate the SM content of the films a Moisture Analyzer, Model MA150 (Goettingen, Germany) was used. Square shaped samples (2 cm × 2 cm) were dried at 105 °C for 120 s. Measurements were then conducted in triplicate for each film system and the results were reported as the average SM (%) ± SD.

2.3.3. Thermogravimetric analysis (TGA) & differential scanning calorimetry (DSC)

A thermal analyzer (Model TGA Q500, Hüllhorst, Germany) was used to carry out the thermogravimetric tests. Samples were heated at a constant rate of 10 °C/min from room temperature up to 600 °C under an air flow of 30 mL/min. Film weights were in the range of 10.8–19.8 mg. Three replicates per sample were analyzed to ensure repeatability. The SDs were lower than 1% for all the systems tested, and the representative curves of each one were reported.

The DSC thermograms were acquired by a DSC Q2000 (Hüllhorst, Germany) and were done in order to evaluate the glass transition and melting temperatures, T_g and T_m, respectively, as well as the enthalpy (ΔH) associated with the amorphous phase and the melting enthalpy (ΔH_m) related to the crystalline phase. Film samples weighing 3.9–4.4 mg were placed individually in aluminum pans and hermetically sealed. An empty pan was used as a reference. Initially, samples were heated at a rate of 10 °C/min from 30 °C to 120 °C under nitrogen atmosphere to remove previous thermal history and moisture (Gutiérrez, Herniou-Julien, Álvarez, & Alvarez, 2018). They were then cooled to −90 °C using an intracooler (TA Refrigerated Cooling Systems 90 - RCS90, Hüllhorst, Germany) and re-heated to 260 °C at a heating rate of 10 °C/min. Two samples of each film system were tested to ensure repeatability. All the thermograms shown refer to the second heating. The ΔH_m was determined from the area under the melting peaks.

2.3.4. Water contact angle (WCA) & surface energy measurements

The water contact angles (WCAs, θ) of the thermo-compressed films were determined by carefully dropping one drop of distilled water (2 μL) onto the thermo-compressed film surfaces using a syringe (KDL Corp., Shanghai, China) and then quickly measuring the WCAs before swelling started with a USB Digital Microscope (contact angle goniometer) model DIGMIC200X (China) equipped with Image Analysis Software 220 × 2.0MP video, at 0.0001° precision, under ambient conditions, i.e. air temperature 25 °C. The WCAs were then calculated from the intersection of the liquid-solid interface (drop of water-surface of the film) and the liquid-vapor interface (tangent to the boundary of the drop) (Gutiérrez & González, 2017). A total of 12 measurements were taken per film and the means ± SD reported.

The bromonaphthalene (BCAs; Sigma Aldrich, 97%, CAS: 90-11-9) and di-iodomethane (DCAs; Sigma Aldrich, 99%, CAS: 15.842-9) contact angles (θ) were also measured, as described above, in order to determine the surface energy of the films. The total surface energy of each sample and their polar and dispersive components were calculated from the equation proposed by Owens (1970):

$$\gamma_L \frac{(1 + \cos\theta)}{2} = (\gamma_S^d \gamma_L^d)^{1/2} + (\gamma_S^p \gamma_L^p)^{1/2} \quad (5)$$

where γ^d and γ^p are the dispersive and polar components of surface free energy, respectively. The subscript S refers to the solid, and L to the liquid, and θ is the contact angle (Gutiérrez & González, 2017). The total surface energy, γ_s, can be estimated by Eq. (6):

$$\gamma_S = \gamma_S^P + \gamma_S^d \quad (6)$$

The surface energy components of probe liquids used for the contact angle measurements are listed in Table 1 (Cyras, Manfredi, Ton-That, & Vázquez, 2008).

2.3.5. Scanning electron microscopy (SEM) of the thermo-compressed and cryo-fractured surface of the films

A JEOL JSM-6460 LV scanning electron microscope was used to analyze the thermo-compressed and cryo-fractured surfaces of the films. Samples were cryo-fractured by freezing them in liquid nitrogen and their morphologies were then observed in the fracture cross-section of the film. For both analyses films were mounted on bronze stubs and sputter-coated (Sputter coater SPI Module, Santa Clara, CA, USA) with a thin layer of gold for 35 s and observed with an accelerating voltage of 15 kV and magnification 1 k×.

Table 1
Total surface energy (γ_l) and their polar (γ_l^P) and dispersive (γ_l^d) components for the liquids used (bromonaphthalene and di-iodomethane) for the calculation of total surface energy (γ_s), and polar (γ_s^P) and dispersive (γ_s^d) components of the different nanocomposite films.

(mN/m)	Bromonaphthalene	Di-iodomethane
γ_l	44.4	50.8
γ_l^P	0.0	2.3
γ_l^d	44.4	48.5

2.3.6. Thickness (e), density (ρ) & opacity (Op)

The *e* of each film system was determined by measuring samples at eighteen random locations per sample using a micrometer (Liuling, Shanghai, China) with an accuracy of ± 0.001 mm. Results were reported as average values ± SD. The thickness results were considered for the calculations of ρ and Op.

Sample discs (12 mm diameter - ø) from each film system were used for ρ determination. The film discs were weighed (W_i), dried at 105 °C for 24 h, and weighed again (W_f). The ρ was then calculated as the ratio between the weight (W) and volume (V) where V is equal to *e* x area (A) of each disc using Eq. (7):

$$\rho = {W}/{V} = {W}/{A*e} = {W_i - W_f}/{\left(\frac{ø}{2}\right)^2 * \Pi * e} \quad (7)$$

The ρ measurements were undertaken in triplicate, and the data reported as mean values ± SD.

The Op of the films was determined following the methodology described by Gutiérrez (2017). The ultraviolet (UV) and visible light barrier properties of the films were measured using a 2800 UV-Vis spectrophotometer (UNICO instruments Co., Ltd., Shangai, China) at selected wavelengths between 400 and 800 nm. Film opacity was then calculated at 600 nm using the equation given by Sukhija, Singh, and Riar (2016):

$$Op = {A_{600}}/{e} \quad (8)$$

where: A_{600} = the absorbance at 600 nm and "*e*" = film thickness (mm).

2.3.7. Uniaxial tensile tests

The mechanical properties of the films were determined from samples cut in a bone-shape with an effective area ~28.6 mm long × ~5.48 mm wide and cross-sectional area ~5.78 mm^2 (the exact values differed slightly between samples). Film samples (10 per formulation) were mounted and clamped with tensile grips (A/TG model) in an INSTRON EMIC 23–50 machine to generate the force-distance curves following the ISO 527-2 (2012) norm. The samples were stretched at a constant speed of 1 mm/s at 21 °C until they broke, using a cell of 50 N.

The overall stress acting on each sample during tension was expressed as the so-called true tensile strength (σ). This is the force normal to the film cross-section *F* (N) divided by the initial area A_0 (m^2) of the sample (Hamann, Zhang, Daubert, Foegeding, & Diehl, 2006):

$$\sigma = {F}/{A_o} \quad (9)$$

The overall strain (ε) of each film was expressed as a percentage of the initial length as follows:

$$\varepsilon\,(\%) = {L}/{L_o} \text{ x } 100 \quad (10)$$

where Lo and L (mm) are the initial and final lengths of each film before and after deformation, respectively.

The mechanical properties at break: maximum stress (σ_m) and strain at break (ε_b) were obtained from the stress-distance curves. For this, the curves were transformed into stress-strain curves as outlined in ISO 527-2 (2012). Young's modulus (*E*) was then determined from the linear regression slope of the stress-strain curves. Toughness (*T*) was calculated from the total area under the stress-strain curves, while the resilience (*R*) of the materials showing creep was determined from the area under the stress-strain curves in the elastic zone.

2.3.8. Biodegradability in vegetable compost & variation in the growth of the primary root of lettuce (Lactuca sativa) seedlings as an ecotoxicity bioassay

The biodegradability of the films developed was determined at 2, 7, 14, 21, 30 days using the protocol described by Gutiérrez (2018b). Biodegradability (%) was calculated as follows:

$$Biodegradability\ (\%) = (W_i - W_f) * W_i^{-1} * 100 \quad (11)$$

where W_i is the initial weight on dry basis of the film before the test and W_f the final dry weight of each film system after the test. The assays were carried out under controlled temperature (25 °C) and RH (70–80%) conditions. Analyses were performed in triplicate and the biodegradability (%) ± SD was reported.

The compostability of the films was determined by first drying samples in an oven at 105 °C for 48 h and then pulverizing each one separately in a grinder to a fine powder. Lettuce (*Lactuca sativa*) seeds were purchased from Cooperativa de Agricultores Mar del Plata (Mar del Plata, Argentina). The seeds were surface-sterilized in 30% commercial bleach and 0.2% Tween 20 for 10 min and then rinsed three times with sterile water. They were then plated on 0.8% Agar-H_2O and placed in a growth chamber at 25 °C with 16 h light photoperiod. Four days post-germination the seedlings were transferred to agar plates containing either H_2O (control) or one of three concentrations of each powdered film system (0.01, 0.1 and 1 mg/mL). After 4 days, the seedlings were photographed and the primary root growth of each was measured using ImageJ image-analysis software (USA National Institute of Health). The values shown are mean values ± SD of three independent experiments. Data are expressed as a percentage of the primary root growth of the control.

2.4. Statistical analyses

The data was analyzed using OriginPro 8 (Version 8.5, Northampton, USA) software. An analysis of variance (ANOVA) was performed for the data obtained from each test. Results are shown as average values ± SD. Differences between the average values of the measured properties were compared using a multiple-range Tukey's test. A significance level of 0.05 was used.

3. Results and discussion

3.1. Attenuated total reflectance Fourier transform infrared (ATR/FTIR) spectroscopy

All the film systems studied showed similar ATR/FTIR spectra (Fig. 1A). A significant absorption peak at around 3300 cm^{-1} associated with the stretching of the OH groups belonging to the starch, glycerol and water, and the stretching vibration of the C-O groups were found in all the systems (Pereira, de Arruda, & Stefani, 2015). The peaks observed at 2857 and 2935 cm^{-1} are associated with C-H stretch vibrations and are characteristic of starch CH_2 groups (Gutiérrez, 2017, 2018a; Mathew, Brahmakumar, & Abraham, 2006). In addition, bands appearing between 1300 and 1430 cm^{-1} were assigned to C-O angular deformations (Gutiérrez & Alvarez, 2017c). Other bands identified were those corresponding to the tension of the C=O groups at 1150 cm^{-1}. The band detected at 1032 cm^{-1} in all the films developed is associated with -C-O-C- glycosidic bonds (Gutiérrez, 2018d). The lack of any differences among the adsorption peaks of the ATR/FTIR spectra of the evaluated films meant that there was no evidence to suggest that the presence of cellulose acetate (C), chromium octanoate as a catalyst (Cat) or a combination of these led to the formation of new (cross-linked) covalent bonds in the thermoplastic starch (TPS)-based materials processed under reactive extrusion (REx) conditions. There were differences, however, in the number of available OH groups among the film systems as estimated using the ratio between the band absorbances at 3300 cm^{-1} (A_{3300}) (Fig. 1B) and 1150 cm^{-1} (A_{1150}) (Fig. 1C) (A_{3300}/A_{1150} ratio) following Shi et al. (2007). The A_{3300}/A_{1150} ratios of the film systems had the following ascending order: TPS + C (0.87) < TPS + Cat (0.89) < TPS + C + Cat (0.94) < TPS (1.05). Thus, the addition of Cat or C, or a combination of both reduced the

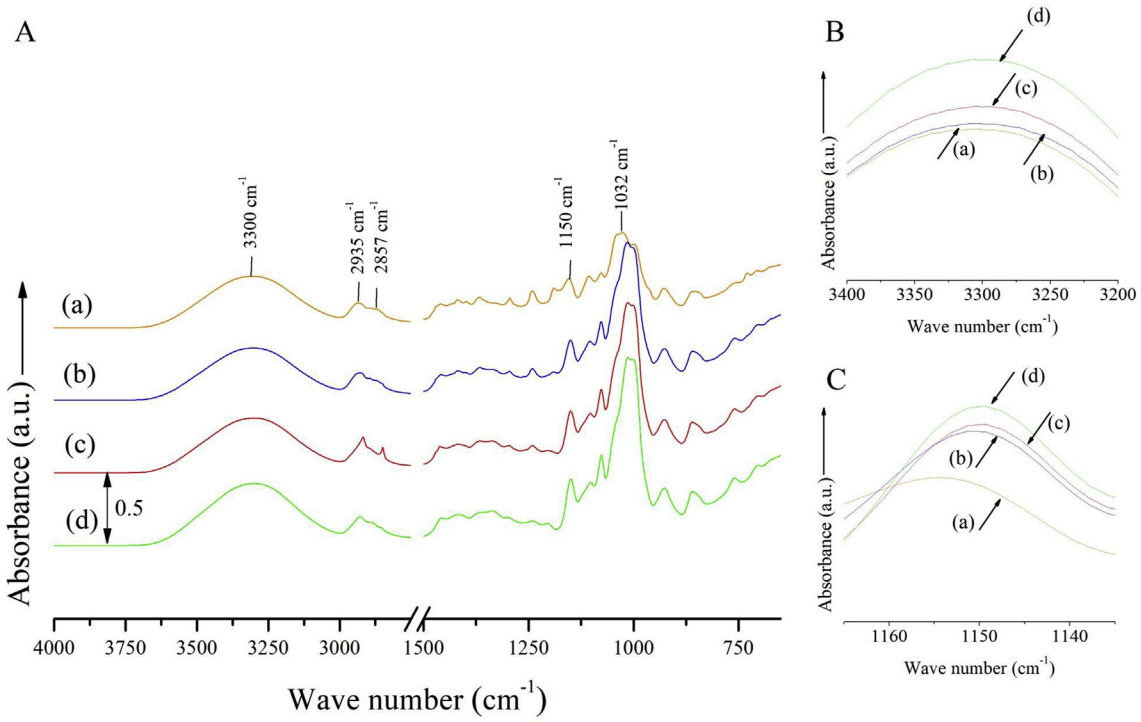

Fig. 1. Panel A- FTIR spectra of the different films studied in all the absorption range. **Panel B**- FTIR spectra in the absorption range corresponding to C-O group (OH stretching) of the different films studied. **Panel C**- FTIR spectra in the absorption range between 1140 cm^{-1} and 1160 cm^{-1}. Film systems: (a) thermoplastic starch (TPS), (b) TPS + cellulose acetate (TPS + C), (c) TPS + catalyst (TPS + Cat) and (d) TPS + C + Cat.

number of available OH groups in the film systems evaluated.

3.2. Moisture content (MC), water solubility (WS), water absorption (WA), swelling (SW) & surface moisture (SM)

The TPS film had the highest MC value (19 ± 1%, Table 2). This is possibly related to the greater number of available OH groups present in the TPS film, which increase its capacity to absorb moisture from the environment. This fits well with the ATR/FTIR spectra analysis. However, this MC value was not significantly higher ($p \geq 0.05$) than the other film systems studied. The TPS + C film had the lowest MC value (17.1 ± 0.9%), but was only significantly lower ($p \leq 0.05$) than the TPS + Cat film (19.0 ± 0.6%, Table 2). This is also in line with the results obtained from the ATR/FTIR spectra.

The TPS film also showed the highest WS value (21.6 ± 0.2%) (Table 2) and the TPS + C film the lowest value (20.7 ± 0.2%), and this difference was statistically significant ($p \leq 0.05$). Otherwise no significant differences in the WS of the films were found. Thus, so far the results suggest that the TPS film is the most hydrophilic system, and the TPS + C film the most hydrophobic system.

The WA values calculated for the films evaluated (approx. 4.2%) at a steady state, i.e. after 24 h, were not statistically different ($p \geq 0.05$, Table 2). Similar results have been reported by Mali, Sakanaka, Yamashita, and Grossmann (2005) for cassava starch-based films.

The TPS + C film had the lowest SW (15.5 ± 0.5%, Table 2), but this was not statistically different ($p \geq 0.05$) from the SWs of the TPS and TPS + C + Cat films. Stronger hydrogen (H)-bonding interactions between the C and the starch chains could have decreased the number of available OH groups in this system, thus reducing its swelling capacity. The TPS + Cat film had the highest SW (24 ± 2%), however, this value was not significantly higher ($p \geq 0.05$) than that of the TPS film (19 ± 4%).

Interestingly, the SM of the TPS + C film (0.84 ± 0.08%, Table 2) was significantly higher (twice as high) ($p \leq 0.05$) compared to the TPS film (0.4 ± 0.1%). These results contrast with the trend observed for the MC values for these same film systems. This suggests that molecular rearrangements occurred within the TPS + C film, which oriented the few available OH groups in this system towards the surface, thus increasing its SM values as compared to the TPS film. It should be noted that there were no statistically significant differences ($p \geq 0.05$) between the SM values of the TPS + C and TPS + Cat film, nor between the SM values of the Cat-containing films (TPS + Cat and TPS + C + Cat) and the TPS film.

Table 2
Moisture content (*MC*), water solubility (*WS*), water absorption (*WA*), swelling (*SW*), surface moisture (*SM*), bromonaphthalene (*BCA*) and di-iodomethane (*DCA*) contact angles, thickness (*e*) and density (ρ) of the different films.

Parameter	TPS	TPS + C	TPS + Cat	TPS + C + Cat
MC (%)	19 ± 1^{a}	17.1 ± 0.9^{a}	19.0 ± 0.6^{a,b}	18.0 ± 0.5^{a}
WS (%)	21.6 ± 0.2^{a,b}	20.7 ± 0.2^{a}	21.2 ± 0.8^{a}	21.0 ± 0.6^{a}
WA (%)	3.8 ± 0.6^{a}	4.8 ± 0.5^{a}	4.0 ± 0.8^{a}	4.4 ± 0.2^{a}
SW (%)	19 ± 4^{a}	15.5 ± 0.5^{a}	24 ± 2^{a,b}	16 ± 3^{a}
SM (%)	0.4 ± 0.1^{a}	0.84 ± 0.08^{b}	1.0 ± 0.8^{a,b}	0.4 ± 0.2^{a}
BCA (°)	42 ± 2^{b}	28.2 ± 0.4^{a}	45 ± 3^{b}	40 ± 2^{b}
DCA (°)	44 ± 2^{b}	40.9 ± 0.9^{a}	50.5 ± 0.6^{c}	51 ± 2^{c}
e (mm)	0.9 ± 0.1^{a}	1.00 ± 0.09^{a}	1.11 ± 0.08^{a,b}	1.18 ± 0.07^{b}
ρ (g/cm^{3})	0.9 ± 0.2^{a,b}	0.76 ± 0.01^{b}	0.9 ± 0.1^{b,c}	0.65 ± 0.07^{a}

Equal letters in the same row indicate no statistically significant differences ($p \leq 0.05$). Film systems: thermoplastic starch (TPS), TPS + cellulose acetate (TPS + C), TPS + catalyst (TPS + Cat) and TPS + C + Cat.

3.3. Thermogravimetric analysis (TGA) & differential scanning calorimetry (DSC)

The TGA curves of the film systems studied (Fig. 2A) show the three stages typical of thermal degradation: 1) the evaporation of adsorbed moisture or free water, 2) the degradation of the starch-rich phase, which also contains glycerol, and 3) the oxidation of the partially decomposed starch (Gutiérrez, Morales, Pérez, Tapia, & Famá, 2015;

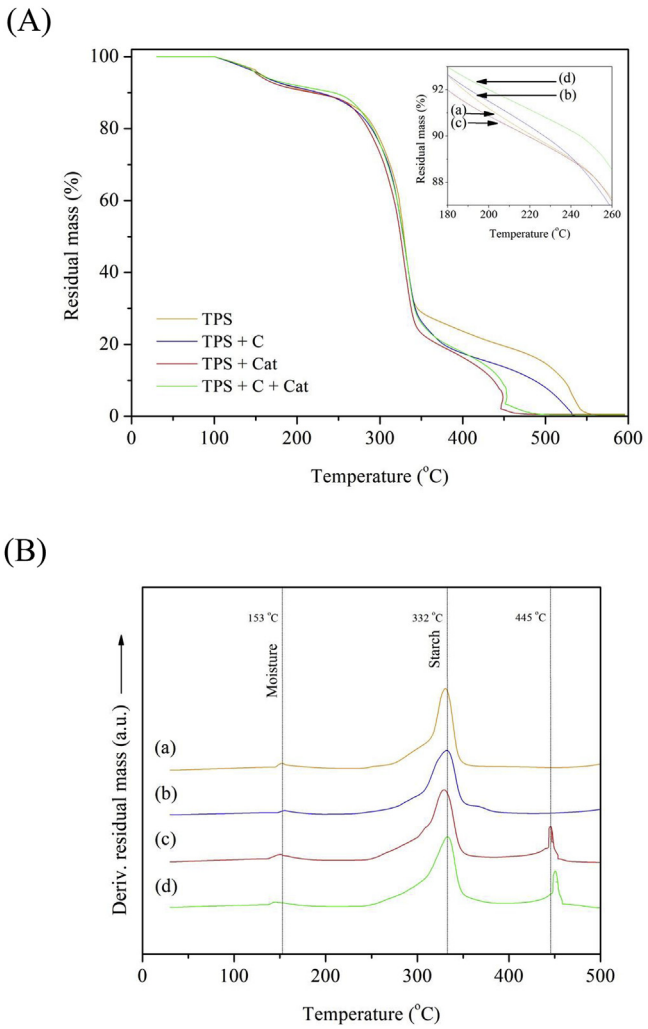

Fig. 2. (A) TGA and (B) DTGA curves of the different films studied: (a) thermoplastic starch (TPS), (b) TPS + cellulose acetate (TPS + C), (c) TPS + catalyst (TPS + Cat) and (d) TPS + C + Cat.

Luchese, Garrido, Spada, Tessaro, & de la Caba, 2018; Luchese, Uranga, Spada, Tessaro, & de la Caba, 2018). It can also be observed from Fig. 2A (see box at the top right of each panel) that the stability of the C-containing films (TPS + C and TPS + C + Cat) was higher than that of the TPS film in the glycerol-rich phase. Similar results were reported by Curvelo, de Carvalho, and Agnelli (2001) for cellulosic fibers/TPS-based composite films. The TPS + C + Cat film showed the highest thermal stability during the glycerol-rich phase. In contrast, the thermal stability of the TPS + Cat film in this phase was lower than that of the TPS film.

The DTGA (derivative TGA) curves (Fig. 2B) of the film systems evaluated showed that none of them exhibited phase separation between the TPS matrix and the glycerol. A maximum evaporation temperature of adsorbed moisture, or free water, was observed at about 153 °C for all the films analyzed. The maximum thermal degradation temperature (T_{max}) of the starch-rich phase was observed at 332 °C, which is comparable to the T_{max} of 317 °C reported for the starch-rich phase in native potato starch-based films plasticized with glycerol (Sessini, Arrieta, Kenny, & Peponi, 2016). It is worth noting that the T_{max} of the starch-rich phase in the TPS + Cat film was slightly lower than that of the other films. This confirms the weakening of the H-bonding interactions between the TPS chains, due to the H-bonding interactions that occurred between the glycerol-starch or Cat-starch molecules.

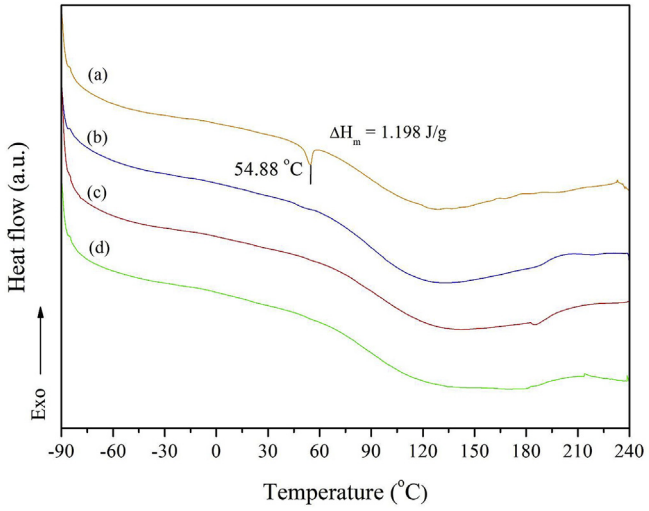

Fig. 3. Heating thermograms of the films based on: (a) thermoplastic starch (TPS), (b) TPS + cellulose acetate (TPS + C), (c) TPS + catalyst (TPS + Cat) and (d) TPS + C + Cat.

Interestingly, other T_{max} peaks were also observed in the Cat-containing film systems (445 °C - TPS + Cat and 450 °C - TPS + C + Cat) (Fig. 2B). These peaks of degradation could be speculatively attributed to the thermal degradation of components with higher molecular weights and thermal resistance, products of the cross-linking of the starch-starch chains and C-starch chains. This speculation is based on the observation that the TGA curve of the Cat (Appendix A) decomposes at a much lower temperature than that of the Cat-containing film systems. Nonetheless, the formation of products resulting from the cross-linking reaction between the starch-starch or C-starch molecules due to the use of the Cat was not confirmed in this study at least not by the analysis of the ATR/FTIR spectra. It is worth noting, however, that there are other results that will be discussed in the following sections, mainly the analysis of the mechanical properties (section 3.6), which also suggest the presence of these products.

From the DSC curves (Fig. 3) a melting peak was observed in the TPS film at 54.88 °C. This has been attributed in the literature to the melting temperature (T_m) of resistant starch (RS) type 3 (RS3, retrograded starch) (Gutiérrez et al., 2018). In contrast, the other film systems did not show melting peaks. Thus, the addition of C, Cat, or the combination of both, led to the production of non-retrograded films. This is a positive result, since retrogradation diminishes film performance (García-Tejeda et al., 2013). As for the amorphous phases of the film systems analyzed, nothing can be said, since glass transition temperatures (T_g) were not observed in any of them.

3.4. Surface energy measurements, water contact angle (WCA) & scanning electron microscopy (SEM) of the thermo-compressed surfaces

The total surface energy of the developed films (γ_s) together with the polar (γ_s^p) and dispersive (γ_s^d) components was calculated from 1) the constants of the solvents used as references: bromonaphthalene and di-iodomethane (Table 1), 2) the values of the bromonaphthalene (*BCA*) and di-iodomethane (*DCA*) contact angles determined experimentally for each film (Table 2), and 3) the equations given in the work of Owens (1970).

According to Aphibanthammakit, Nigen, Gaucel, Sanchez, and Chalier (2018) films made from biopolymers have bipolar surface properties, i.e. the total surface energy of the films depends on the energy provided by the polar and dispersive (no polar) components of the material surface. This is in line with the results obtained here: both the polar and dispersive components contributed to the total surface energy for all the film systems. The highest value of the polar

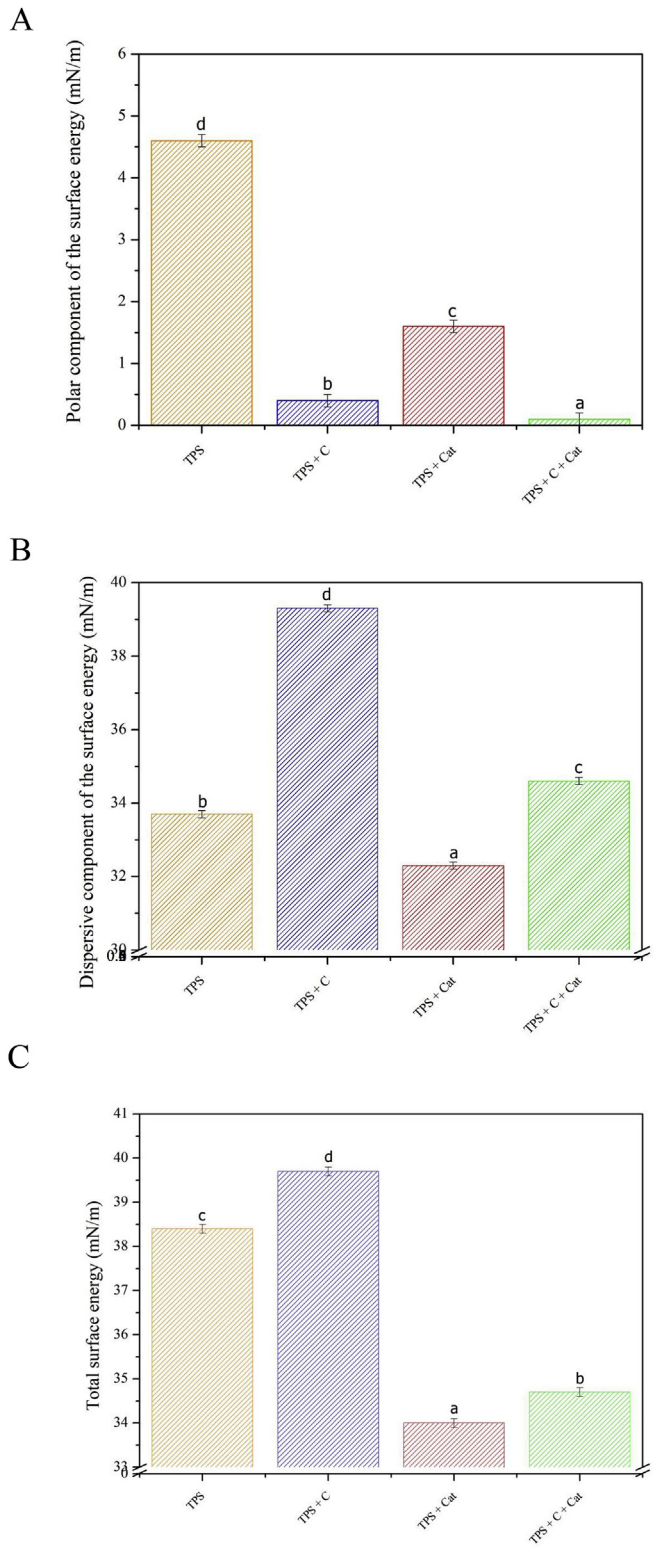

Fig. 4. Panel A- Values of the polar component of the surface energy. **Panel B**- Values of the dispersive component of the surface energy. **Panel C**- Values of total surface energy of the different films studied. Film systems: thermoplastic starch (TPS), TPS + cellulose acetate (TPS + C), TPS + catalyst (TPS + Cat) and TPS + C + Cat. Equal letters in the columns indicate no statistically significant differences ($p \leq 0.05$).

component was registered for the TPS film (4.6 ± 0.1 mN/m, Fig. 4A) which fits well with the fact that it was also the most hydrophilic of the films studied. In contrast, the highest value of the dispersive component was recorded for the TPS + C film (39.3 ± 0.1 mN/m, Fig. 4B). This would also be in line with the results previously analyzed as the TPS + C film was the most hydrophobic material. The total surface energy values for the developed films varied from 34.0 ± 0.1 mN/m to 39.7 ± 0.1 mN/m (Fig. 4C) for the TPS + Cat and TPS + C films, respectively. Our research group has observed in the past that an increase in the total surface energy of starch-based films is related to an increase in the WCA values (Gutiérrez & González, 2017). This is because the strong H-bonding interactions that occur below the surface of the material restrict the more polar sites (Lewis sites) thus increasing the WCA values and the hydrophobicity of the surface. In this study, however, the WCA results (Fig. 5) did not correlate well with the total surface energy values, since the highest WCA value was observed for the TPS + C + Cat film (81 ± 1°), while the TPS, TPS + C and TPS + Cat films had average WCA values of around 72° and there were no statistically significant differences ($p \geq 0.05$) among them. Wenzel (1936) suggested that higher WCA values in films made from biopolymers may be related to a rougher surface. This roughness can create physical obstacles that prevent the collapse of the water drop, consequently reducing the wetting of the film surface. This would fit well with the results reported in this study as the TPS + C + Cat film exhibited a rougher surface morphology (Fig. 6) than the other systems analyzed. These results suggest that physical aspects of the film surface can have an influence on WCA values that is similar to, or greater than, the chemical aspects of film systems.

3.5. Thickness (e), density (ρ) & opacity (Op)

The films containing the additives tended to be thicker than the TPS film (Table 2). The Cat-containing films (TPS + Cat and TPS + C + Cat), however, were the only ones that were significantly thicker ($p \leq 0.05$) than the TPS film.

All the films gave ρ values between 0.65 and 0.9 g/cm^3 (Table 2). Similar ρ values have been reported by Gutiérrez (2018d) for films prepared from sagu (*Canna edulis* Kerr) starch (0.75 ± 0.07 g/cm^3) and flour (0.68 ± 0.04 g/cm^3), and processed by blending/thermomolding. In this study, the films containing the additives tended to be less dense than the TPS film, although the densities of the TPS and TPS + Cat films were not statistically different ($p \geq 0.05$). The TPS + C + Cat film (0.65 ± 0.07 g/cm^3) was the least dense material, followed by the TPS + C film (0.76 ± 0.01 g/cm^3). It is also worth noting that there was an inverse trend between the e and ρ values of the TPS film and the films containing the additives.

The e values, in general, affect the Op values of starch films (Sukhija et al., 2016). This behavior was not, however, evident in this study. Op values varying from 0.6 to 0.9 were observed for the developed films (Fig. 7) but there were no statistically significant differences ($p \geq 0.05$) among them. Nevertheless, the Cat-containing films did tend to be more opaque. This could be due to the rougher surface morphology shown by these materials (Fig. 6). It is well known that rougher surface morphologies partially scatter light, which is then less easily transmitted through the material, thus increasing its opacity (Gutiérrez, 2017; Gutiérrez & González, 2017; Gutiérrez, Suniaga, Monsalve, & García, 2016). The Cat-containing films (TPS + Cat and TPS + C + Cat) were also darker than the TPS and TPS + C films (Fig. 7).

3.6. Scanning electron microscopy (SEM): cryo-fractured surface analysis & uniaxial tensile tests

The cryo-fractured surfaces of the films analyzed (Fig. 6) exhibited similar amorphous morphologies without any evidence of microstructures such as starch granules. This shows that the REx conditions selected to process the blends ensured complete starch gelatinization. Cryo-fractured surface morphologies are frequently associated with the mechanical behavior of materials. This relationship was not observed in

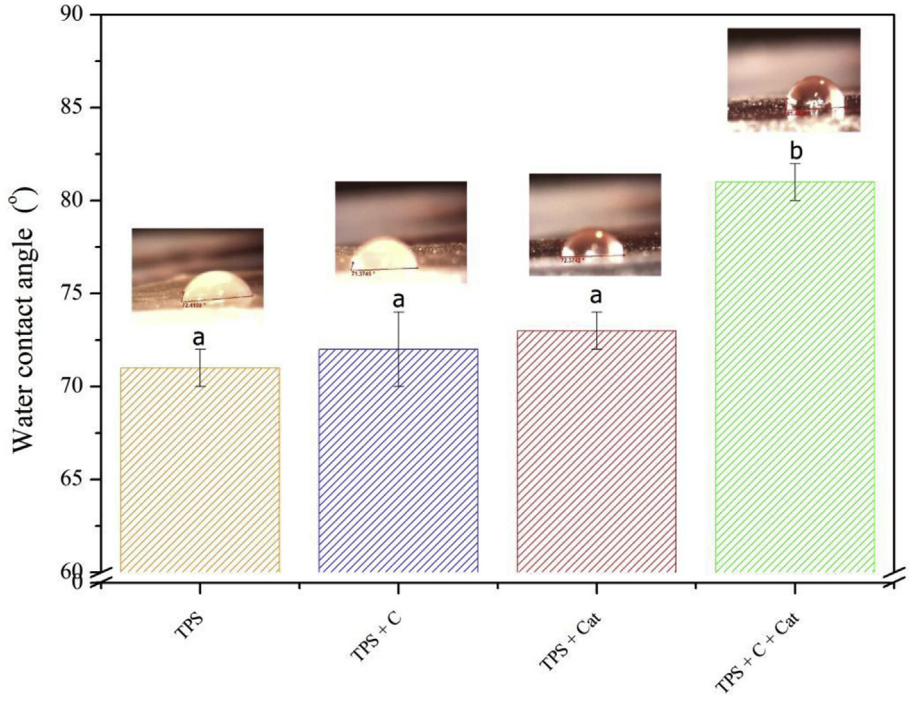

Fig. 5. Values (°) and images of water contact angles (WCA) of the films based on: thermoplastic starch (TPS), TPS + cellulose acetate (TPS + C), TPS + catalyst (TPS + Cat) and TPS + C + Cat. Equal letters in the columns indicate no statistically significant differences ($p \leq 0.05$).

this study, however, as the morphologies of the films in the cryo-fracture zone were so similar.

Nonetheless, the mechanical behavior of the analyzed films was interesting (Fig. 8A), as the Cat-containing films (TPS + Cat and TPS + C + Cat) showed a small localized creep zone between 5.02% and 5.84% of strain and between 0.43 MPa and 0.45 MPa of stress, with elastic behavior before the creep zone, and plastic behavior after it. In contrast, the films without the Cat were almost totally plastic. This mechanical behavior has also been observed by our research group for cross-linked films prepared from corn starch/polystyrene blends and plantain flour/poly(ε-caprolactone) (PCL) blends using zinc octanoate (1.9%) and zirconium octanoate (3.3%) as catalysts, respectively

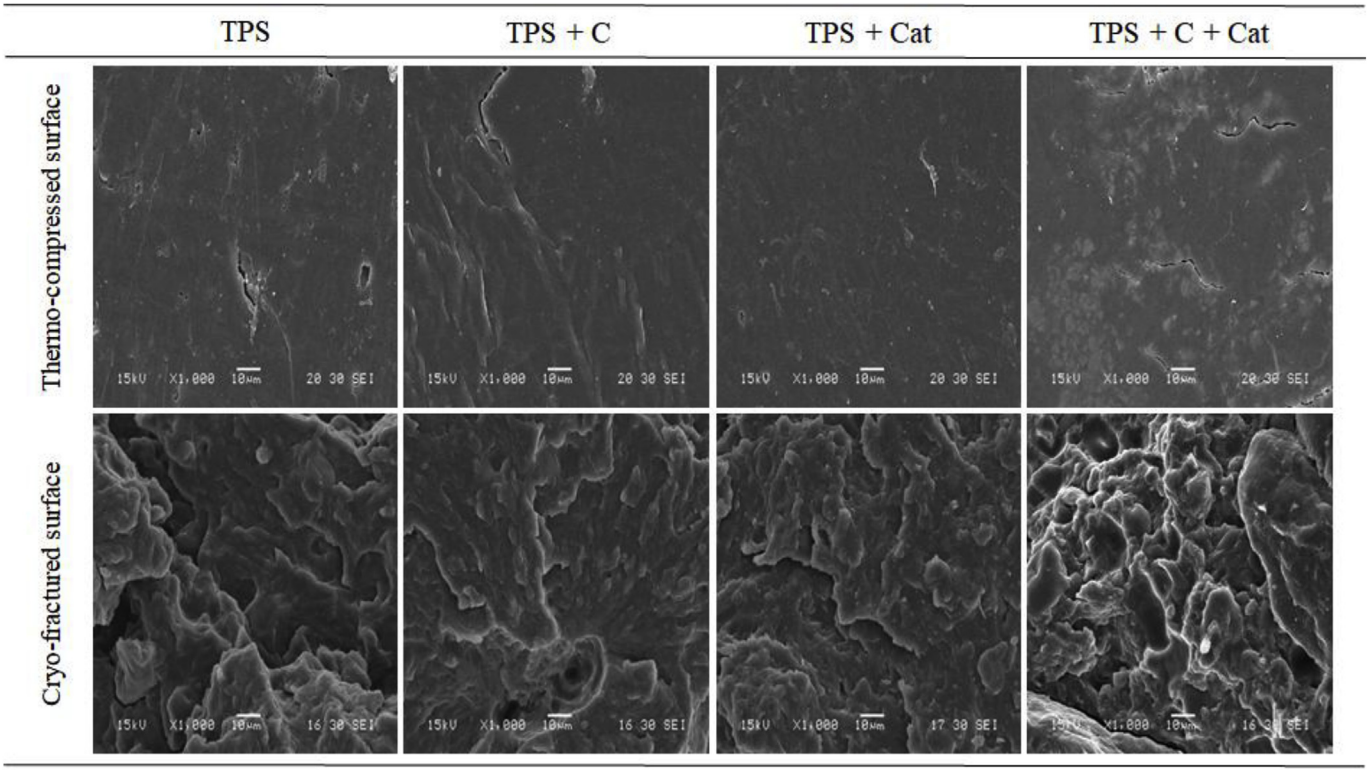

Fig. 6. SEM micrographs of the thermo-compressed surface and the cryo-fractured surface of the films based on: thermoplastic starch (TPS), TPS + cellulose acetate (TPS + C), TPS + catalyst (TPS + Cat) and TPS + C + Cat. At 1.0 k× of magnification.

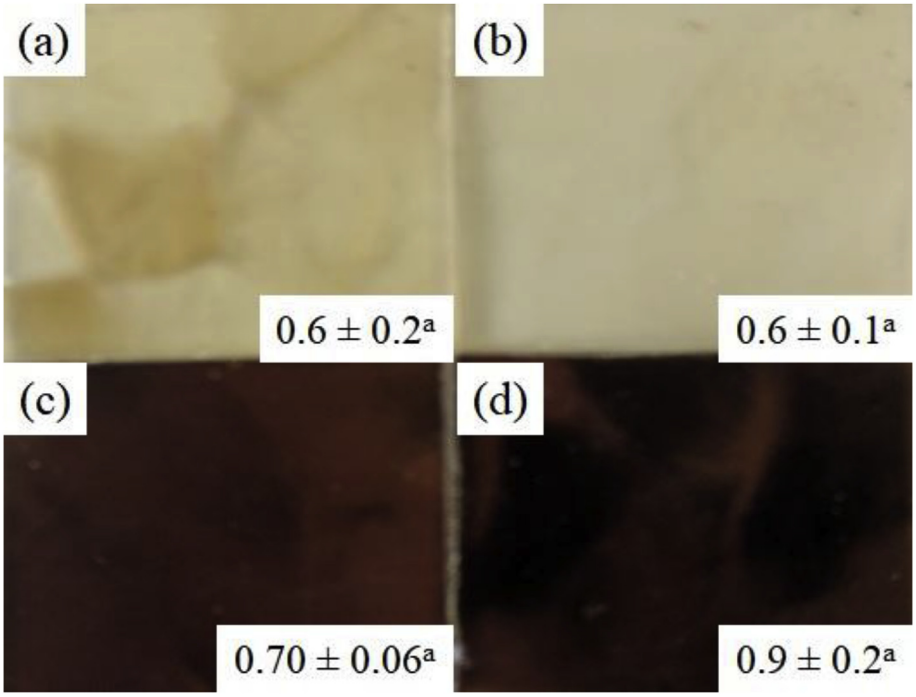

Fig. 7. Appearance and opacity (*Op*) values of the films based on: (a) thermoplastic starch (TPS), (b) TPS + cellulose acetate (TPS + C), (c) TPS + catalyst (TPS + Cat) and (d) TPS + C + Cat. Equal subindex letters indicate no statistically significant differences ($p \leq 0.05$).

(Gutierrez & Alvarez, 2017a; 2017b, 2017c). Thus, although there was no structural evidence to demonstrate the cross-linking of the Cat-containing films in this study, the results do suggest that it might, in fact, have occurred.

According to Gutiérrez and Alvarez (2017c) after the creep zone Hooke's Law for elastic, linear and isotropic materials is not met. This means that normal deformation does not occur anywhere in the solid, nor along any of the directions of the normal stresses in the orthogonal axes, i.e. the principal directions of the stress matrix do not coincide with the principal direction of the matrix of deformation. In addition, the positive slopes of the curves in the plastic deformation range for the Cat-containing films implies that hardening occurs until the sample finally breaks. This could be associated with the parallel alignment of the polymer chains to the load (Gutiérrez & Alvarez, 2017b) and fits well with the cross-linking mechanisms suggested for the Cat-containing film systems.

It is worth noting that for different food packaging applications, the duration of stress, temperature and applied load should also be considered as the mechanical behavior observed for the Cat-containing films means that these materials would fail in a kinematic system (Gutiérrez & Alvarez, 2017c).

Theoretically, deformation is reversible for materials experiencing creep, as long as the stress-strain conditions do not exceed the elastic zone of the material. Once the stress-strain conditions of the elastic zone reach a certain threshold, however, changes in the volume and shape of the material are irreversible (Gutiérrez & Alvarez, 2017b, 2017c). Taking these considerations into account Auad, Contos, Nutt, Mirta, and Marcovich (2008) and Auad et al. (2012) investigated the development of nanocellulose-reinforced shape memory polyurethane films. The Cat-containing film systems studied here could be proposed as food packaging materials with shape memory, as long as the following mechanical thresholds are not reached 5.02% strain and 0.43 MPa stress. It should be noted that although these mechanical conditions are very poor this research does open a window to study and develop food packaging with shape memory derived from bio-based polymers through easily industrialized processing conditions. With this in mind, Sessini, Arrieta, Fernández-Torres, and Peponi (2018) also reported a humidity-activated shape memory effect on plasticized starch-based films for biomedical and food packaging applications.

All the maximum stress (σ_m) values for the films containing the additives were statistically higher ($p \leq 0.05$) than the σ_m for the TPS film (Fig. 8B). As expected, the addition of C led to an increase in the σ_m of around 146% compared to the TPS film, i.e. from 0.6 MPa to 0.88 MPa for the TPS and TPS + C films, respectively. Similar mechanical behavior was reported by Müller, Laurindo, and Yamashita (2009) for cassava starch-based films with concentrations of cellulose fiber varying from 0.10 to 0.50 g fibers/g starch. The highest σ_m value was recorded for the TPS + Cat film (1.35 ± 0.03 MPa). The addition of Cat to the TPS matrix resulted in an increase in the σ_m value of about 2.25 times compared to the TPS film. In general, the σ_m values tended to be higher in Cat-containing films than the TPS films. Similar results were observed by Gutiérrez and Alvarez (2017b) for films prepared from plantain flour/PCL blends under REx conditions using zirconium octanoate as a catalyst.

The values of strain at break (ε_b) were statistically higher ($p \leq 0.05$) in the films containing the additives compared to the TPS film (Fig. 8C). The most plastic material was the TPS + Cat film (ε_b = 15.8 ± 0.9%). This could be related to the stronger H-bonding interactions between the glycerol (plasticizer)-starch or Cat-starch molecules, as observed from the TGA results (see section 3.3). The ε_b values also increased by between 160% and 187% for the TPS + C and TPS + C + Cat films, respectively, as compared to the TPS film, i.e. both the addition of C and Cat led to an increase in the ε_b values.

Young's modulus (E) values ranged from 0.239 to 0.256 MPa for the films analyzed (Fig. 8D). The C-containing films tended to have higher E values than the TPS film. No statistically significant differences ($p \geq 0.05$), however, were observed. In contrast, adding cellulose fibers to cassava starch films did produce statistically significant variations in the E values at concentrations as low as 0.10 g fibers/g starch (Müller et al., 2009).

The toughness (T) of a material reflects its ability to absorb energy before reaching break point. Polymeric films with high T values are desirable as food packaging materials as they can absorb the energy of any knocks or bumps that occur during food transportation and storage

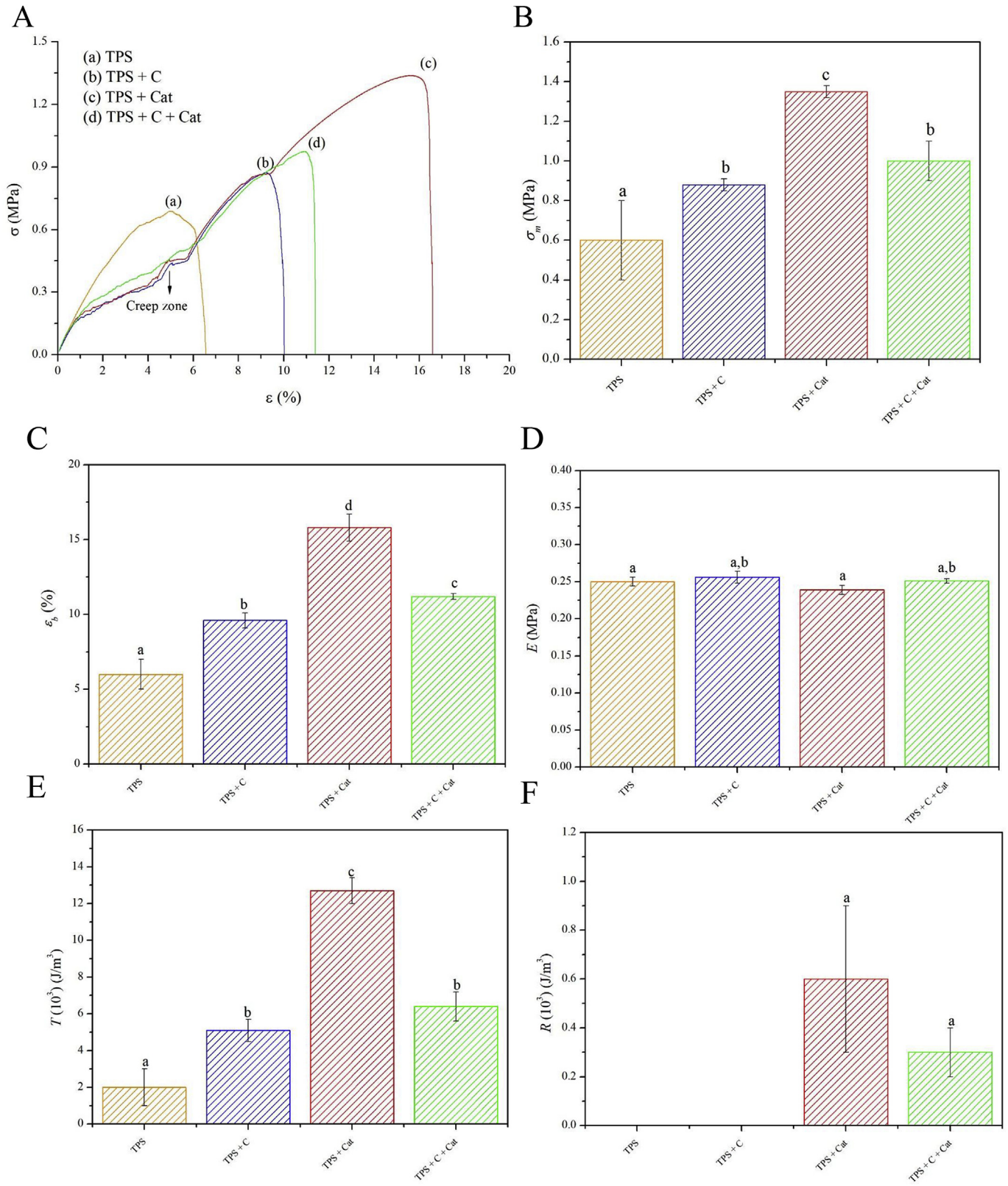

Fig. 8. Panel A- Stress (σ)-strain (ε) curves of the films. **Panel B**- Maximum stress (σ_m) values. **Panel C**- Values of strain at break (ε_b). **Panel D**- Young's modulus (E) values. **Panel E**- Toughness (T) values. **Panel F**- Resilience (R) values. Film systems: (a) thermoplastic starch (TPS), (b) TPS + cellulose acetate (TPS + C), (c) TPS + catalyst (TPS + Cat) and (d) TPS + C + Cat. Equal letters in the columns indicate no statistically significant differences ($p \leq 0.05$).

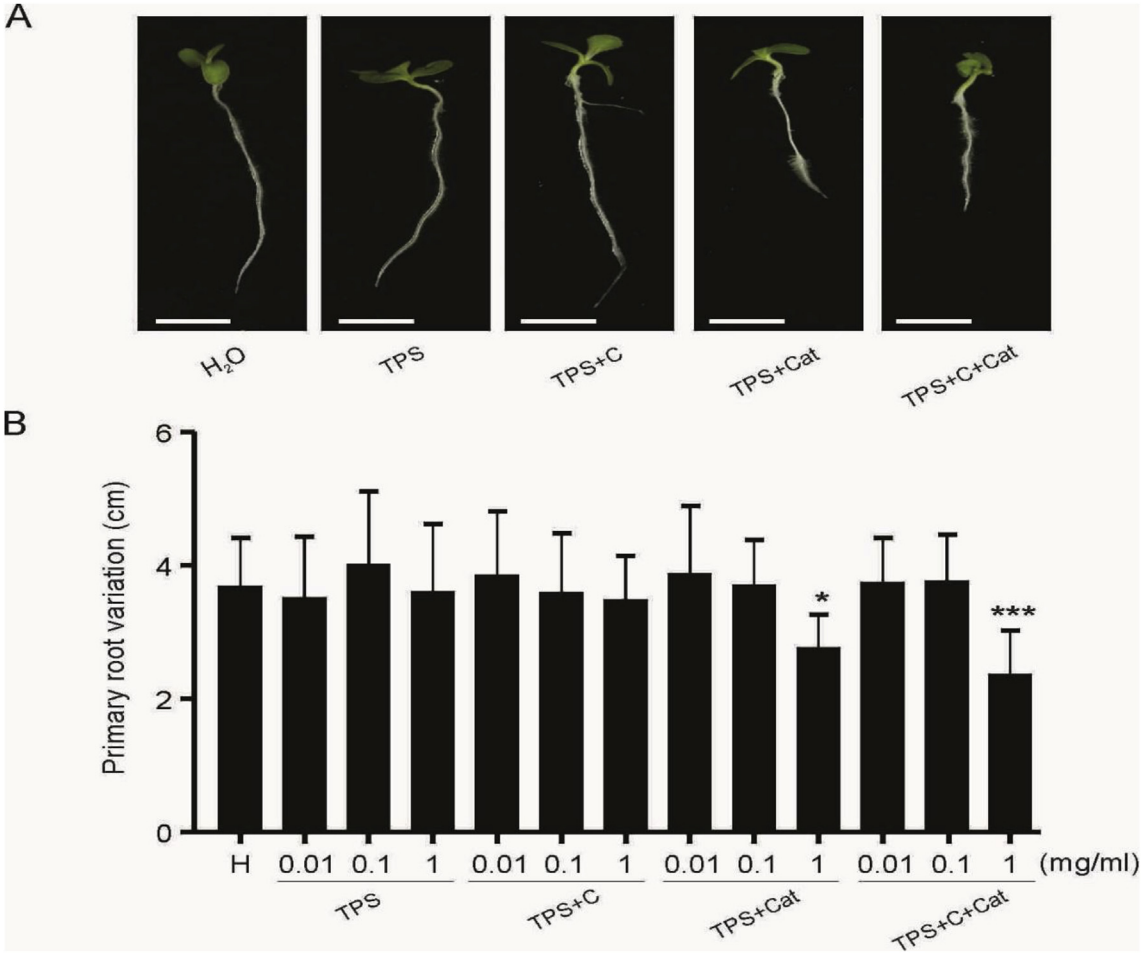

Fig. 9. Compostability study of each analyzed film system using the primary root variation (%) in lettuce (*Lactuca sativa*) seedlings germinated on 0.8% agar-H_2O in Petri plates. **Panel A**- Representative image of the lettuce seedlings treated with each film systems at a concentration of 1 mg/mL (Bars = 1 cm). **Panel B**- Measurement of primary root variation in lettuce seedlings at different film concentrations: 0.01, 0.1 and 1 mg/mL. The data are expressed as a percentage with respect to the control system (TPS film). Values are the mean (± SD) of three independent experiments. Statistical analysis was performed by one-way ANOVA analysis of variance; *p* values of less than 0.05 were considered as statistically significant (Tukey's Test). $*p < 0.05$, $***p < 0.001$. Film systems: thermoplastic starch (TPS), TPS + cellulose acetate (TPS + C), TPS + catalyst (TPS + Cat) and TPS + C + Cat.

(Gutiérrez, 2018a). With this in mind, the TPS + Cat film was the most tenacious material, and the TPS film the least tenacious material (Fig. 8E). Intermediate *T* values were observed for the C-containing film systems (TPS + C and TPS + C + Cat). The TPS + Cat film systems could therefore be of interest to the food industry as a food packaging material.

It is well known that only those materials with creep have resilience (*R*). In this study only the Cat-containing films showed this mechanical property, with *R* values between 0.3 and 0.6 × 10^3 J/m^3 (Fig. 8F). No statistically significant differences ($p \geq 0.05$) in these *R* values were observed between the Cat-containing films. Despite this, the TPS + Cat films tended to show higher *R* values than the TPS + C + Cat films.

In general, all the mechanical parameters examined were improved by the addition of the composites. The TPS + Cat film, in particular, was the material that showed the best mechanical performance.

3.7. Biodegradability in vegetable compost & variation in the growth of the primary root of lettuce (Lactuca sativa) seedlings as an ecotoxicity bioassay

Studies of biodegradability and compostability have been little studied in TPS-based films, since many authors have presumed that the native or modified starch matrices and additives added intentionally to reinforce the polymer matrix do not cause any harm to the environment. Our research group, however, has recently shown that it is not only important that these TPS-based materials are biodegradable, but also that they are compostable, i.e. they must disintegrate to reduced particle sizes, and these particles should not cause ecotoxic damage (Gutiérrez, 2018b). In this study we did not find any statistically significant differences ($p \geq 0.05$) in the biodegradability of the film systems tested over the experimentation period (90 days). In fact, after 90 days all the materials studied had completely (100%) biodegraded.

In order to evaluate the compostability of the manufactured materials and determine their potential ecotoxic effect, known amounts of the developed films were added as composting materials for seedlings of a well-known food crop, lettuce (*Lactuca sativa*). Interestingly, we observed that the length of the primary roots of the seedlings planted with a concentration of 1 mg/mL of the TPS + Cat and TPS + C + Cat films (Fig. 9) were significantly shorter ($p \leq 0.05$) than the roots of the seedlings planted using the other film systems without Cat (TPS and TPS + C) as composting materials. This led us to reach the following conclusion: the accumulation of these materials, especially the Cat-containing film systems, could have a negative impact on the vegetation giving them a limited compostability rating in spite of the fact that they are biodegradable.

Finally, more in-depth studies should be conducted to determine the compostability of films derived from Cat-containing food hydrocolloids in order to answer the following questions: 1) is their ecotoxicity in soil systems reversible or irreversible? and 2) even when seedling root

growth is not affected could the Cat be incorporated, concentrated, and maintained in the seedlings?

4. Conclusions

Food hydrocolloid blends made from cellulose acetate (C)/corn starch processed under reactive extrusion (REx) conditions were well characterized and analyzed in order to evaluate their compostability and potential cross-linking interactions. This study was not able, however, to satisfactorily structurally determine whether cross-linking occurred between the C-starch chains or starch-starch chains under REx conditions, with or without the addition of chromium octanoate as a catalyst (Cat). Despite this, the films made from the Cat-containing food hydrocolloid blends gave other results that did suggest that cross-linking might have taken place. The Cat-containing films were biodegradable but non-compostable. Interestingly, the Cat-containing film systems showed creep and resilience and thus have potential for the development of shape-memory food packaging materials.

Conflicts of interest

The authors declare no conflict of interest.

Acknowledgements

The authors would like to thank the Consejo Nacional de Investigaciones Científicas y Técnicas (CONICET) (Postdoctoral fellowship internal PDTS-Resolution 2417), Universidad Nacional de Mar del Plata (UNMdP) and Université de Bretagne-Sud (grant 10428) for financial support. We would also like to thank Dr. Mirian Carmona-Rodríguez for her valuable contribution. Many thanks also to Andres Torres Nicolini for all the assistance he provided during this study.

Appendix A. Supplementary data

Supplementary data to this article can be found online at https://doi.org/10.1016/j.foodhyd.2018.10.024.

References

Aphibanthammakit, C., Nigen, M., Gaucel, S., Sanchez, C., & Chalier, P. (2018). Surface properties of Acacia *Senegal* vs Acacia *seyal* films and impact on specific functionalities. *Food Hydrocolloids, 82*, 519–533. https://doi.org/10.1016/j.foodhyd.2018.04.032.

Association of Official Analytical Chemists (AOAC) (1990). *Official methods of analysis*.

Auad, M. L., Contos, V. S., Nutt, S., Mirta, A. I., & Marcovich, N. E. (2008). Characterization of nanocellulose-reinforced shape memory polyurethanes. *Polymer International, 57*(4), 651–659. https://doi.org/10.1002/pi.2394.

Auad, M. L., Richardson, T., Hicks, M., Mosiewicki, M. A., Aranguren, M. I., & Marcovich, N. E. (2012). Shape memory segmented polyurethanes: Dependence of behavior on nanocellulose addition and testing conditions. *Polymer International, 61*(2), 321–327. https://doi.org/10.1002/pi.3193.

Chevalier, E., Assezat, G., Prochazka, F., & Oulahal, N. (2018). Development and characterization of a novel edible extruded sheet based on different casein sources and influence of the glycerol concentration. *Food Hydrocolloids, 75*, 182–191. https://doi.org/10.1016/j.foodhyd.2017.08.028.

Curvelo, A. A. S., de Carvalho, A. J. F., & Agnelli, J. A. M. (2001). Thermoplastic starch–cellulosic fibers composites: Preliminary results. *Carbohydrate Polymers, 45*(2), 183–188. https://doi.org/https://doi.org/10.1016/S0144-8617(00)00314-3.

Cyras, V. P., Manfredi, L. B., Ton-That, M.-T., & Vázquez, A. (2008). Physical and mechanical properties of thermoplastic starch/montmorillonite nanocomposite films. *Carbohydrate Polymers, 73*(1), 55–63. https://doi.org/10.1016/j.carbpol.2007.11.014.

Dai, X., Xiong, Z., Ma, S., Li, C., Wang, J., Na, H., et al. (2015). Fabricating highly reactive bio-based compatibilizers of epoxidized citric acid to improve the flexural properties of polylactide/microcrystalline cellulose blends. *Industrial & Engineering Chemistry Research, 54*(15), 3806–3812. https://doi.org/10.1021/ie504904c.

Dai, X., Xiong, Z., Na, H., & Zhu, J. (2014). How does epoxidized soybean oil improve the toughness of microcrystalline cellulose filled polylactide acid composites? *Composites Science and Technology, 90*, 9–15. https://doi.org/https://doi.org/10.1016/j.compscitech.2013.10.009.

Dhar, P., Tarafder, D., Kumar, A., & Katiyar, V. (2016). Thermally recyclable polylactic acid/cellulose nanocrystal films through reactive extrusion process. *Polymer, 87*, 268–282. https://doi.org/https://doi.org/10.1016/j.polymer.2016.02.004.

Dogu, B., & Kaynak, C. (2016). Behavior of polylactide/microcrystalline cellulose biocomposites: Effects of filler content and interfacial compatibilization. *Cellulose, 23*(1), 611–622. https://doi.org/10.1007/s10570-015-0839-0.

FDA (2016). *Indirect additives used in food contact substances.* Retrieved from https://www.accessdata.fda.gov/scripts/fdcc/index.cfm?set=IndirectAdditives&id=STANNOUSETHYLHEXANOATE.

García-Tejeda, Y. V., López-González, C., Pérez-Orozco, J. P., Rendón-Villalobos, R., Jiménez-Pérez, A., Flores-Huicochea, E., et al. (2013). Physicochemical and mechanical properties of extruded laminates from native and oxidized banana starch during storage. *Lebensmittel-Wissenschaft und -Technologie- Food Science and Technology, 54*(2), 447–455. https://doi.org/10.1016/j.lwt.2013.05.041.

Gutiérrez, T. J. (2017). Effects of exposure to pulsed light on molecular aspects of edible films made from cassava and taro starch. *Innovative Food Science & Emerging Technologies, 41*, 387–396. https://doi.org/10.1016/j.ifset.2017.04.014.

Gutiérrez, T. J. (2018a). Active and intelligent films made from starchy sources/blackberry pulp. *Journal of Polymers and the Environment, 26*(6), 2374–2391. https://doi.org/10.1007/s10924-017-1134-y.

Gutiérrez, T. J. (2018b). Are modified pumpkin flour/plum flour nanocomposite films biodegradable and compostable? *Food Hydrocolloids, 83C*, 397–410. https://doi.org/https://doi.org/10.1016/j.foodhyd.2018.05.035.

Gutiérrez, T. J. (2018c). Biodegradability and compostability of food nanopackaging materials. In G. Cirillo, M. A. Kozlowski, & U. G. Spizzirri (Eds.). *Composites materials for food packaging* (pp. 269–296). Wiley. https://doi.org/10.1002/9781119160243.ch9.

Gutiérrez, T. J. (2018d). Biological macromolecule composite films made from sagu starch and flour/poly(ε-caprolactone) blends processed by blending/thermo molding. *Journal of Polymers and the Environment, 26*(9), 3902–3912. https://doi.org/10.1007/s10924-018-1268-6.

Gutiérrez, T. J., & Alvarez, V. A. (2017a). Data on physicochemical properties of active films derived from plantain flour/PCL blends developed under reactive extrusion conditions. *Data in Brief: 15*, (pp. 445–448). . https://doi.org/10.1016/j.dib.2017.09.071.

Gutiérrez, T. J., & Alvarez, V. A. (2017b). Eco-friendly films prepared from plantain flour/PCL blends under reactive extrusion conditions using zirconium octanoate as a catalyst. *Carbohydrate Polymers, 178*, 260–269. https://doi.org/10.1016/j.carbpol.2017.09.026.

Gutiérrez, T. J., & Alvarez, V. A. (2017c). Properties of native and oxidized corn starch/polystyrene blends under conditions of reactive extrusion using zinc octanoate as a catalyst. *Reactive and Functional Polymers, 112*, 33–44. https://doi.org/10.1016/j.reactfunctpolym.2017.01.002.

Gutiérrez, T. J., & Alvarez, V. A. (2018). Bionanocomposite films developed from corn starch and natural and modified nano-clays with or without added blueberry extract. *Food Hydrocolloids, 77*, 407–420. https://doi.org/10.1016/j.foodhyd.2017.10.017.

Gutiérrez, T. J., & González, G. (2017). Effect of cross-linking with *Aloe vera* gel on surface and physicochemical properties of edible films made from plantain flour. *Food Biophysics, 12*(1), 11–22. https://doi.org/10.1007/s11483-016-9458-z.

Gutiérrez, T. J., González Seligra, P., Medina Jaramillo, C., Famá, L., & Goyanes, S. (2017a). Effect of filler properties on the antioxidant response of thermoplastic starch composites. In V. K. Thakur, M. K. Thakur, & M. R. Kessler (Vol. Eds.), *Handbook of composites from renewable materials, structure and chemistry. Vol. 1. Handbook of composites from renewable materials, structure and chemistry* (pp. 337–370). John Wiley & Sons. https://doi.org/10.1002/9781119441632.ch14.

Gutiérrez, T. J., Guarás, M. P., & Alvarez, V. A. (2017b). Reactive extrusion for the production of starch-based biopackaging. In M. A. Masuelli (Ed.). *Biopackaging*Miami: CRC Press, Taylor & Francis Group. Retrieved from https://www.crcpress.com/Biopackaging/Masuelli/p/book/9781498749688.

Gutiérrez, T. J., Herniou-Julien, C., Álvarez, K., & Alvarez, V. A. (2018). Structural properties and in vitro digestibility of edible and pH-sensitive films made from Guinea arrowroot starch and wastes from wine manufacture. *Carbohydrate Polymers, 184*, 135–143. https://doi.org/10.1016/j.carbpol.2017.12.039.

Gutiérrez, T. J., Morales, N. J., Pérez, E., Tapia, M. S., & Famá, L. (2015). Physico-chemical properties of edible films derived from native and phosphated cush-cush yam and cassava starches. *Food Packaging and Shelf Life: 3*, (pp. 1–8). . https://doi.org/10.1016/j.fpsl.2014.09.002.

Gutiérrez, T. J., Suniaga, J., Monsalve, A., & García, N. L. (2016). Influence of beet flour on the relationship surface-properties of edible and intelligent films made from native and modified plantain flour. *Food Hydrocolloids, 54*, 234–244. https://doi.org/10.1016/j.foodhyd.2015.10.012.

Hamann, D. D., Zhang, J., Daubert, C. R., Foegeding, E. A., & Diehl, K. C. (2006). Analysis of compression, tension and torsion for testing food gel fracture properties. *Journal of Texture Studies, 37*(6), 620–639. https://doi.org/10.1111/j.1745-4603.2006.00074.x.

ISO 527-2 (2012). Determination of tensile properties of plastics. Retrieved from https://www.iso.org/obp/ui/#iso:std:56046:en.

Khoo, R. Z., & Chow, W. S. (2017). Mechanical and thermal properties of poly(lactic acid)/sugarcane bagasse fiber green composites. *Journal of Thermoplastic Composite Materials, 30*(8), 1091–1102. https://doi.org/10.1177/0892705715616857.

Kowalski, A., Duda, A., & Penczek, S. (1998). Kinetics and mechanism of cyclic esters polymerization initiated with tin(II) octoate, 1. Polymerization of ε-caprolactone. *Macromolecular Rapid Communications, 19*(11), 567–572. https://doi.org/10.1002/(SICI)1521-3927(19981101)19:11%0c567::AID-MARC567%0e3.0.CO;2-T.

Liu, F., Avena-Bustillos, R. J., Chiou, B.-S., Li, Y., Ma, Y., Williams, T. G., et al. (2017). Controlled-release of tea polyphenol from gelatin films incorporated with different ratios of free/nanoencapsulated tea polyphenols into fatty food simulants. *Food Hydrocolloids, 62*, 212–221. https://doi.org/10.1016/j.foodhyd.2016.08.004.

Liu, H., Xie, F., Yu, L., Chen, L., & Li, L. (2009). Thermal processing of starch-based polymers. *Progress in Polymer Science, 34*(12), 1348–1368. https://doi.org/https://doi.org/10.1016/j.progpolymsci.2009.07.001.

Luchese, C. L., Garrido, T., Spada, J. C., Tessaro, I. C., & de la Caba, K. (2018a). Development and characterization of cassava starch films incorporated with blueberry pomace. *International Journal of Biological Macromolecules, 106*, 834–839. https://doi.org/https://doi.org/10.1016/j.ijbiomac.2017.08.083.

Luchese, C. L., Uranga, J., Spada, J. C., Tessaro, I. C., & de la Caba, K. (2018b). Valorisation of blueberry waste and use of compression to manufacture sustainable starch films with enhanced properties. *International Journal of Biological Macromolecules, 115*, 955–960. https://doi.org/https://doi.org/10.1016/j.ijbiomac.2018.04.162.

Ludueña, L., Vázquez, A., & Alvarez, V. (2012). Effect of lignocellulosic filler type and content on the behavior of polycaprolactone based eco-composites for packaging applications. *Carbohydrate Polymers, 87*(1), 411–421. https://doi.org/https://doi.org/10.1016/j.carbpol.2011.07.064.

Mali, S., Sakanaka, L. S., Yamashita, F., & Grossmann, M. V. E. (2005). Water sorption and mechanical properties of cassava starch films and their relation to plasticizing effect. *Carbohydrate Polymers, 60*(3), 283–289. https://doi.org/https://doi.org/10.1016/j.carbpol.2005.01.003.

Mathew, S., Brahmakumar, M., & Abraham, T. E. (2006). Microstructural imaging and characterization of the mechanical, chemical, thermal, and swelling properties of starch–chitosan blend films. *Biopolymers, 82*(2), 176–187. https://doi.org/10.1002/bip.20480.

Morán, J. I., Vázquez, A., & Cyras, V. P. (2013). Bio-nanocomposites based on derivatized potato starch and cellulose, preparation and characterization. *Journal of Materials Science, 48*(20), 7196–7203. https://doi.org/10.1007/s10853-013-7536-x.

Morelli, C. L., Belgacem, N., Bretas, R. E. S., & Bras, J. (2016). Melt extruded nanocomposites of polybutylene adipate-co-terephthalate (PBAT) with phenylbutyl isocyanate modified cellulose nanocrystals. *Journal of Applied Polymer Science, 133*(34) https://doi.org/10.1002/app.43678.

Müller, C. M. O., Laurindo, J. B., & Yamashita, F. (2009). Effect of cellulose fibers addition on the mechanical properties and water vapor barrier of starch-based films. *Food Hydrocolloids, 23*(5), 1328–1333. https://doi.org/10.1016/j.foodhyd.2008.09.002.

Owens, D. K. (1970). Some thermodynamic aspects of polymer adhesion. *Journal of Applied Polymer Science, 14*(7), 1725–1730. https://doi.org/10.1002/app.1970.070140706.

Pereira, V. A., de Arruda, I. N. Q., & Stefani, R. (2015). Active chitosan/PVA films with anthocyanins from *Brassica oleraceae* (Red Cabbage) as time–temperature indicators for application in intelligent food packaging. *Food Hydrocolloids, 43*, 180–188. https://doi.org/10.1016/j.foodhyd.2014.05.014.

Sessini, V., Arrieta, M. P., Fernández-Torres, A., & Peponi, L. (2018). Humidity-activated shape memory effect on plasticized starch-based biomaterials. *Carbohydrate Polymers, 179*, 93–99. https://doi.org/https://doi.org/10.1016/j.carbpol.2017.09.070.

Sessini, V., Arrieta, M. P., Kenny, J. M., & Peponi, L. (2016). Processing of edible films based on nanoreinforced gelatinized starch. *Polymer Degradation and Stability, 132*, 157–168. https://doi.org/https://doi.org/10.1016/j.polymdegradstab.2016.02.026.

Shi, R., Zhang, Z., Liu, Q., Han, Y., Zhang, L., Chen, D., et al. (2007). Characterization of citric acid/glycerol co-plasticized thermoplastic starch prepared by melt blending. *Carbohydrate Polymers, 69*(4), 748–755. https://doi.org/10.1016/j.carbpol.2007.02.010.

Sukhija, S., Singh, S., & Riar, C. S. (2016). Analyzing the effect of whey protein concentrate and psyllium husk on various characteristics of biodegradable film from lotus (*Nelumbo nucifera*) rhizome starch. *Food Hydrocolloids, 60*, 128–137. https://doi.org/10.1016/j.foodhyd.2016.03.023.

Toro-Márquez, L. A., Merino, D., & Gutiérrez, T. J. (2018). Bionanocomposite films prepared from corn starch with and without nanopackaged Jamaica (*Hibiscus sabdariffa*) flower extract. *Food and Bioprocess Technology, 11*(11), 1955–1973. https://doi.org/10.1007/s11947-018-2160-z.

Wenzel, R. N. (1936). Resistance of solid surfaces to wetting by water. *Industrial and Engineering Chemistry, 28*(8), 988–994. https://doi.org/10.1021/ie50320a024.

Yu, L., Dean, K., & Li, L. (2006). Polymer blends and composites from renewable resources. *Progress in Polymer Science, 31*(6), 576–602. https://doi.org/10.1016/j.progpolymsci.2006.03.002.

Zhang, X., & Zhang, Y. (2016). Reinforcement effect of poly(butylene succinate) (PBS)-grafted cellulose nanocrystal on toughened PBS/polylactic acid blends. *Carbohydrate Polymers, 140*, 374–382. https://doi.org/https://doi.org/10.1016/j.carbpol.2015.12.073.